Cement & Concrete Composites 60 (2015) 135–145

Contents lists available at ScienceDirect

Cement & Concrete Composites

journal homepage: www.elsevier.com/locate/cemconcomp

Acoustic emission waveform characterization of crack origin and mode in fractured and ASR damaged concrete

Yaghoob Farnam [a,*], Mette Rica Geiker [b], Dale Bentz [c], Jason Weiss [a]

[a] Lyles School of Civil Engineering, Purdue University, 550 Stadium Mall Dr., West Lafayette, IN 47907, USA
[b] Department of Structural Engineering, Norwegian University of Science and Technology, 7491 Trondheim, Norway
[c] Materials and Structural Systems Division, National Institute of Standards and Technology, 100 Bureau Drive, Stop 8615, Gaithersburg, MD 20899, USA

ARTICLE INFO

Article history:
Received 11 August 2014
Received in revised form 6 April 2015
Accepted 9 April 2015
Available online 18 April 2015

Keywords:
Acoustic emission
Aggregate
Alkali silica reaction
Concrete
Fracture
Matrix

ABSTRACT

Different constituents of concrete can have cracking behavior that varies in terms of the acoustic waveform that is generated. Understanding the waveform may provide insight into the source and behavior of a crack that occurs in a cementitious composite. In this study, passive acoustic emission (AE) was used to investigate the waveform properties of the individual components of concrete (i.e., aggregate, paste, and interfacial transition zone (ITZ)). First, acoustic events produced by cracks generated using mechanical loading in a wedge splitting test were detected. It was observed that cracks that occurred through the aggregate have an AE frequency range between 300 kHz and 400 kHz, while cracks that propagated through the matrix (paste and ITZ) have a frequency range between 100 kHz and 300 kHz. Second, tests were performed using samples that were susceptible to alkali silica reaction; and AE and X-ray computed tomography were used to detect cracking. AE events with a frequency range between 300 kHz and 400 kHz were detected at early ages, suggesting the initiation of cracks within reactive aggregate. At later ages, AE events were detected with frequency ranges of 100–300 kHz, indicating crack development and propagation in the matrix.

1. Introduction

The basic premise of this paper is that a heterogeneous composite system like concrete can develop cracking behavior that is dependent on the properties of the constituent components. It is known that as concrete is loaded, microcracks form initially and eventually these microcracks will propagate, coalesce, and serve as a source for the development of a localized, visible crack [1,2]. Over the last four decades, numerous techniques have been used to better understand concrete fracture. These methods include (but are not limited to) visual observation, optical microscopic examination, scanning electron microscopy, X-ray computed tomography, ultrasonic pulse velocity, resonant frequency, and acoustic emission [3–9]. Attempts have been made to identify the cause of cracking and to pinpoint the location at which cracking is taking place [3–8].

Among several techniques used to detect concrete fracture, acoustic emission (AE) is a real-time, non-invasive testing technique that has been used by many researchers to investigate the fracture processes in concrete [10–19]. Passive AE refers to sound waves that are produced when a material undergoes cracking; and it is based on the principle that when a crack develops in a material, energy is released and a portion of this energy is dissipated as an acoustic wave possessing different frequencies. Acoustic waves and corresponding energy could be released by the generation of cracks or microcracks under several types of internal or external loading [20]. The characteristics of the generated acoustic waves (e.g., the number of counts, number of hits, amplitude, rise time, duration, velocity, frequency, signal strength, and corresponding AE energy) may provide a means to identify the constituents that fracture in the concrete. The strength of the signals and the waveform properties of the signal generally depend on the amount of released energy, distance, source, orientation of the source with respect to the AE sensor, and the nature of the transferring medium [10,20–22]. When AE is performed in a passive mode, AE transducers continuously capture acoustic waves generated by the formation of cracks or microcracks during a test. These acoustic waves are then analyzed to identify the type and magnitude of the resulting damage [23–27].

Materials with different microstructures and mechanical properties produce different types of acoustic activity when they undergo cracking [28]. Analyzing AE signals can therefore help to

* Corresponding author.
E-mail addresses: yfarnam@purdue.edu (Y. Farnam), mette.geiker@ntnu.no (M.R. Geiker), dale.bentz@nist.gov (D. Bentz), wjweiss@purdue.edu (J. Weiss).

http://dx.doi.org/10.1016/j.cemconcomp.2015.04.008
0958-9465/

determine the type and severity of the damage [8,10,12,25,29–31]. Since AE can provide a continuous measurement of crack formation and can detect its waveform properties, it may provide an improvement in understanding fundamental mechanisms in concrete fracture.

In the present study, passive acoustic emission measurements are utilized to determine whether the cracking can be assigned to the individual constituent components of the concrete in which the cracks likely occur. In cementitious materials, the source of these activities is located either in the aggregate or the matrix (cement paste and interfacial transition zone (ITZ)). The waveform of an AE event generated at different sources in the concrete can have distinguishable properties due to the nature and mechanical properties of its source. The aim of this work is to characterize the fracture behavior of the concrete by analyzing the AE waveforms and to thus identify the fracture behavior of the individual components of the concrete (i.e., aggregate and matrix). Once the AE waveform characteristics of each component are defined, they can be used to detect the time and the source of cracking in concrete.

2. Experimental program

To study the fracture behavior of different components in concrete, two types of experiments are performed including mechanical and chemical testing. In the first part of this study, the mechanical wedge splitting test is used to determine AE waveform signatures of cracking by changing the material in which the cracking occurs. Aggregate, cement paste, and ITZ are designed to be cracked individually, thereby knowing the constituent material in which the cracking is generated. The second part of this paper investigates alkali–silica reaction (ASR) of concrete using reactive and non-reactive aggregates. Cracks caused by ASR appear to develop inside aggregate as tensile cracks first before they extend to ITZ and cement paste as tensile and shear cracks [32–34]. The AE results of ASR cracking are compared to the waveform properties of the constituent components obtained in the first part of this study. X-ray computed tomography is also carried out on ASR samples at different exposure ages to further define the fracture behavior of ASR cracking. Table 1 shows the experimental program that was carried out in this study.

2.1. Wedge splitting test

2.1.1. Materials, mixture proportioning, specimen preparation and conditioning

Mortar and paste were prepared using ordinary Portland cement (Alborg Portland CEM II/A-LL52.5) in a standard mixer in accordance with NT BUILD 201 [35]. Granite rock from Bornholm, Denmark was used as aggregate with a maximum aggregate size of 4.75 mm. The specimen geometry was based on standard cube specimens (100 mm on a side) provided with a cast groove and a sawn starter notch (Fig. 1). The depth of the starter notch was equal to half of the specimen depth. The width of the notch was 5 mm [36,37]. A wet saw was used to create the notch while the sample was supported properly.

Four series of samples were prepared for subsequent wedge splitting tests. In the first series, the wedge splitting test was performed on mortar samples made with different water-to-cement ratios by mass (w/c) of 0.32, 0.42, and 0.50; it was assumed that as the w/c of the mortar increased, more cracking would occur through paste and ITZ (mortar matrix), while mortar with a lower w/c has cracking through not only matrix, but also aggregate. In the second series, bulk pieces of granite rock were cut and prepared using the wedge splitting test sample size noted above. In the third series, specimens were prepared using only cement paste with w/c of 0.34 by mass. In the fourth series, the split sections of granite rocks obtained after performing the wedge splitting test in the second series were used to prepare paste-rock samples; these half rock and half paste samples were prepared to simulate the interfacial transition zone (ITZ) in concrete. To prepare the fourth series, a half piece of rock was placed in the mold and the other half space of the mold was cast using a paste with w/c of 0.42. Specimens were kept in limewater for 20 d (20 °C ± 1 °C) after demolding and were removed from the limewater 1 h prior to starting the test.

2.1.2. Testing procedure

The wedge splitting test was performed in accordance with NT BUILD 511 [37] as shown in Fig. 1. The specimen was equipped with a groove and a starter notch (to ensure the crack propagation)

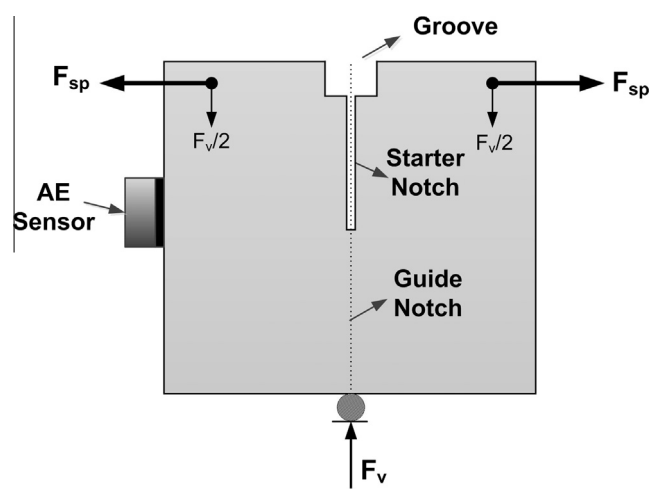

Fig. 1. Fracture wedge splitting test of concrete equipped with AE sensor.

Table 1
Experimental program.

Experiment	Test type	Sample type	Purpose
Wedge splitting and AE measurement	Series 1: mortar	w/c = 0.32, .042, and 0.50	Influence of w/c on cracking behavior of mortar samples
	Series 2: granite rock	–	Determination of waveform signature for aggregate cracking
	Series 3: cement paste	w/c = 0.32	Determination of waveform signature for paste cracking
	Series 4: half rock and half paste	w/c for paste = 0.32	Determination of waveform signature for ITZ cracking
Alkali silica reaction	Length change measurement	Mortar bar with w/c = 0.47 made with reactive and non-reactive sand	Determination of length change due to ASR in mortar sample
	AE measurement	Mortar cylinder with w/c = 0.47 made with reactive and non-reactive sand	Determination of waveform signature for aggregate and matrix cracking due to ASR in mortar sample
	X-ray computed tomography	Mortar cylinder with w/c = 0.47 made with reactive and non-reactive sand	Determination of cracking pattern and damage development due to ASR in mortar sample

(Fig. 1). Two steel brackets with roller bearings were placed partly on top of the specimen and partly into the groove, and through a wedging device, the splitting force (F_{sp}) was applied. During the test, the load in the vertical direction (F_v) and the crack opening displacement (COD) were monitored.

After the specimen was placed in the loading device, it was preloaded to a level of 50–100 N. Thereafter, in the beginning of the test, the measured COD increased at a constant rate of 25–50 μm/min for COD from 0 mm to 0.2 mm. For COD between 0.2 mm and 2 mm, a constant rate of 0.25 mm/min was applied. When the COD passed 2 mm, the rate of loading increased to 0.5 mm/min. The load–COD diagram was determined by continuously measuring and logging corresponding values of the vertical load (F_v) and the COD. The splitting force (F_{sp}) can then be calculated using Eq. (1).

$$F_{sp} = \frac{F_v}{2\tan(\alpha)} \tag{1}$$

where $\langle\alpha\rangle$ is the angle between the wedge and the vertical load line. During testing, an acoustic emission sensor was attached to the end of the cube using Dow high vacuum grease. [1]The sensor was held in contact with the specimen using a rubber band, to record acoustic activity during fracturing.

In this study, a Vallen AMSY5[1] acoustic emission system with the capability of wave transient recording (TR) was used. Therefore, a complete waveform diagram of any captured wave was recorded and then analyzed. VS375-M cylindrical broadband sensors with a diameter of 20.3 mm and a height of 14.3 mm were used. This type of transducer is a broadband frequency transducer with its peak sensitivity at 375 kHz and is ideally suited for detecting waves due to crack growth in noisy environments. During testing, the acoustic waves generated due to the crack/microcrack formation were captured by the AE sensor and then converted to electrical signals. The electrical signals were processed and magnified by preamplifiers. A data acquisition system with the capability of streaming TR data up to 10 MHz was used to record the results. A noise threshold of 40 dB was considered for all AE sensors to exclude surrounding environmental noise.

2.2. Alkali silica reaction test

Three series of experiments were prepared for subsequent alkali silica reaction test. In the first series, length changes of mortar bars were measured similar to the procedure described in ASTM C1260-07 [38], however, the mortar specimens were cured for two weeks and the experiment was carried out at 23 °C ± 2 °C. In the second series, cylindrical mortar specimens were exposed to 1 N NaOH solution and the acoustic emission activities that were caused by either aggregate or matrix cracking were measured. In the third series, X-ray computed tomography was performed on cylindrical samples which were exposed to 1 N NaOH solution; and damage development and cracking were monitored.

2.2.1. Materials, mixture proportioning, specimen preparation and conditioning

Mortar specimens were prepared using ordinary Portland cement (OPC, Type I) with a *w/c* of 0.47 by mass and 55% fine aggregate by volume. The total equivalent alkali content of the cement was 0.86%, including 0.35% of sodium oxide and 0.77% of potassium oxide, by mass. Reactive aggregates (Jobe sand, Texas [20]) and non-reactive aggregates (ASTM Ottawa standard sand [39]) were used. These two aggregates had relatively similar particle size distributions. The sieve analysis for the reactive and non-reactive aggregates was determined according to ASTM C136-06 [40] and is shown in Fig. 2. According to ASTM C136-06 [40], the maximum standard deviation for the sieve analysis test is less than 1% for a single-operator measurement. The mortar made using the cement and the reactive fine aggregates showed more than 0.1% expansion after 3 d, 0.67% after 14 d, and 0.81% after 28 d when tested according to ASTM C1260-07 at 80 °C ± 2 °C [20,38].

The mortar was prepared in a standard mortar mixer in accordance with ASTM C305-12 [41]. ASTM C490 standard mortar prisms [42] with square cross section of 25 mm × 25 mm and length of 285 mm were prepared for length expansion testing. Extra mortar prisms were prepared for X-ray computed tomography evaluations. For the AE experiment, smaller cylindrical samples were cast, since it has been shown that ASR cracking can be detected using AE techniques in specimens with different dimensions [20]. The AE samples were 20 mm in diameter and 40 mm in height and were cast in a plastic form. The length change and the X-ray computed tomography samples were cast in steel molds.

One day after casting, the samples were removed from their molds and sealed in a double plastic sheet and maintained at 23 °C ± 1 °C for two weeks for curing. Samples were then soaked in water for one day at 23 °C ± 1 °C. After immersing in water, samples were immersed in a 1 N NaOH solution at 23 °C ± 1 °C; and length change of mortar bars and AE tests of cylindrical samples were performed. The volume proportion of sodium hydroxide solution to mortar samples in a storage container was 4 ± 0.5 volumes of solution to 1 volume of mortar samples.

Cylindrical X-ray computed tomography samples with a diameter of 10 mm and a height of 25 mm were prepared by coring from extra prismatic samples after two weeks curing. A jeweler's diamond bit (inner diameter of 10.28 mm) was used with center core water pressure to keep the core intact. After coring, these samples were immersed in water and then moved to a 1 N NaOH solution with a similar conditioning as was done for the other samples.

2.2.2. Acoustic emission detection

During the ASR test, one AE sensor was used to continuously record passive AE signals; this was done due to the small size of the cylindrical samples. The AE sensors used in this study had a sensitivity of −75 ± 13 dB re 1 V/μbar to detect AE activity within the frequency range between 75 kHz and 500 kHz. Fig. 3a shows the experimental setup for AE detection for ASR testing. A small container was used; a hole was made in the container lid with the same diameter as the ASR sample. Then, the cylindrical sample was inserted inside the container through the hole in such a manner that the flat end of the cylindrical sample was kept at the same level

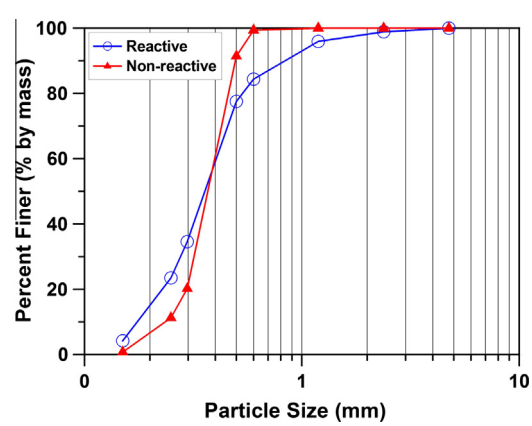

Fig. 2. Sieve analysis for reactive and non-reactive aggregate.

[1] Certain commercial products are identified in this paper to specify the materials used and procedures employed. In no case does such identification imply endorsement or recommendation by the National Institute of Standards and Technology or Purdue University, nor does it indicate that the products are necessarily the best available for the purpose.

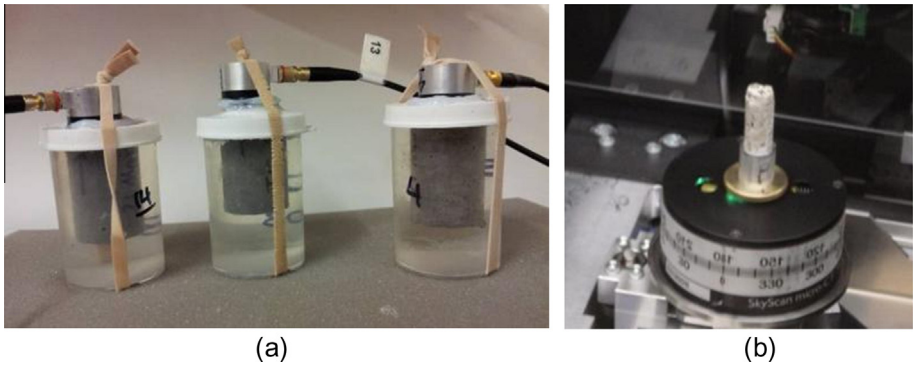

Fig. 3. (a) Mortar sample immersed in 1 N NaOH for ASR test with AE sensor, (b) mortar core sample inside X-ray computed tomography instrument to detect cracks.

(plane) as the container lid (Fig. 3a). This was done to attach the AE sensor. A rubber gasket was used between the sample and the hole on the container lid to tighten and seal the sample inside the container. Afterward, 1 N NaOH solution was injected inside the container using a syringe through a very small hole that had been established in the container lid earlier. Passive AE detection was begun immediately after the container was filled by the 1 N NaOH solution. The AE sensor was installed using a chemical resistant bearing grease (MOLYKOTE 3451 Dow Corning grease1). This grease is resistant to harsh chemicals or solvents, and high and low temperatures. A slight force was applied to the sensor using a rubber band to have a better contact at the sensor/sample interface. All containers were placed on a sound and vibration dampening mat to reduce the surrounding noise. The acoustic emission equipment that was used is the same as that used for the wedge splitting tests.

2.2.3. X-ray computed tomography

X-ray computed tomography was performed using a SkyScan 1172[1] system on 10 mm diameter samples. Fig. 3b illustrates the sample on the turntable in the SkyScan 1172 unit. To scan the samples, the samples were removed from the 1 N NaOH solution and the bottom portion of the sample (in surface saturated dry (SSD) condition) was fitted into an aluminum sleeve. Before exposure to sodium hydroxide, initial radiographs were taken that were subsequently converted into tomographic reconstructed images. During ASR experiments, tomography was performed at different exposure times (i.e., 13 d, 22 d, 37 d, 44 d, 66 d, 89 d, 116 d, and 168 d) to monitor initiation and growth of cracks. At every imaging, multiple scans were performed in the vertical direction (averaging of 4 images at each angle, with an angular spacing of 0.3 degrees) and reassembled for a single tomography dataset, using a camera detector with 4000 pixels × 4000 pixels. For the sample sizes, the 10 mm diameter sample had each voxel representing approximately 3.9 μm × 3.9 μm × 3.9 μm. An aluminum filter with 0.5 mm thickness was used to reduce the low energy X-rays; and the X-ray source was typically operated at 93 keV and 108 mA.

3. Experimental results and discussions

3.1. Wedge splitting test

3.1.1. Typical mechanical and acoustic emission response for concrete

Fig. 4 indicates the typical mechanical response and AE energy for concrete with different *w*/*c*. While the load–COD curve has a similar linear pre-peak response for different *w*/*c*, the peak load increases as *w*/*c* decreases. The differences in load–COD curves between samples with different *w*/*c* occur when the load levels exceeds 70% of peak load. In this region, the stress concentration in the mortar becomes large enough to initiate the coalescence of micro cracking. With increasing load, cracks continue to coalesce until crack localization and propagation occur during the post-peak softening [43].

Regarding the AE activity illustrated in Fig. 4, all samples showed a relatively similar trend in AE energy release. Before peak load, AE energy increases with a higher rate which can be attributed to formation of microcracks, coalescence, and localization of micro/macro cracking. The amount of AE energy released before peak load is less than 10% of the total AE energy that was released at a 1 mm COD (which is nearly complete cracking and damage of the sample with very little remaining load capacity (Fig. 4)). During the initial loading a relatively low amount of AE energy has been generated. This AE energy can be due to the formation of small microcracks with a relatively low amount of new surface area

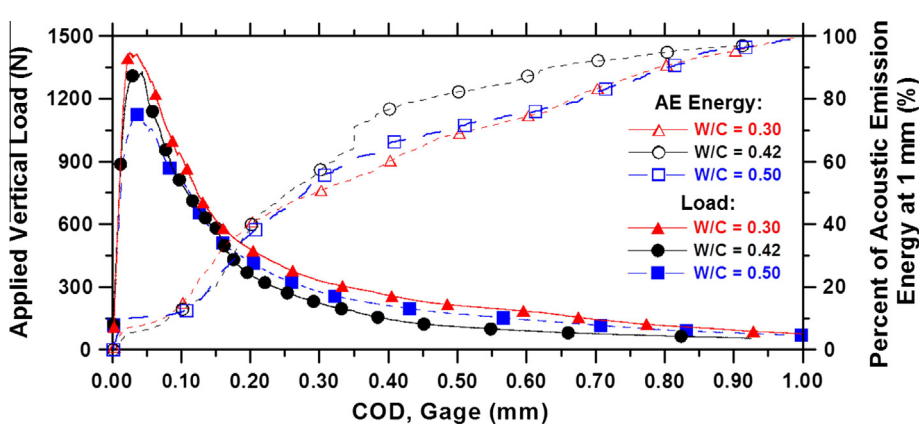

Fig. 4. Load and percent of acoustic emission energy versus crack opening displacement for different *w*/*c* (AE measurement had a coefficient of variation (COV) equal to 21% on total acoustic energy, and fracture properties had an average COV equal to 24%).

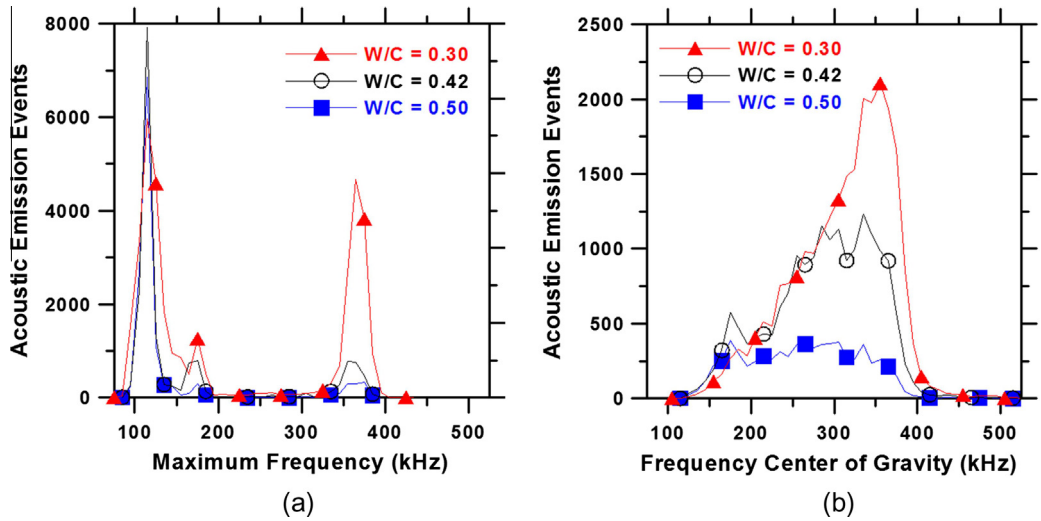

Fig. 5. Properties of acoustic emission waveforms in cracking of concrete with different *w*/*c*: (a) distribution of acoustic emission events versus maximum frequency and (b) distribution of acoustic emission events versus frequency center of gravity.

created. After the peak load is reached, the AE energy increases at a higher rate, which can be attributed to crack propagation (macro crack growth and crack opening). The rate of AE energy increase reduces as the COD reaches 1 mm, indicating that the sample reaches nearly complete failure.

3.1.2. Acoustic waveform analysis of mechanical fracture in concrete

During crack coalescence, localization and propagation, the ITZ and paste strength play an important role in the fracture of concrete [43]. For concrete with higher *w*/*c*, the paste has a relatively lower strength due to a higher porosity [44,45]. The matrix (ITZ and paste) is weaker than aggregates and most of the cracks occur in this component [43]. In concrete with very low *w*/*c*, the matrix strength increases. Accordingly, cracking begins to occur more frequently in the aggregate, which implies that cracking in higher strength concrete occurs in the aggregate and the matrix. Therefore, it is expected that for concrete with higher *w*/*c*, the captured acoustic events during a splitting test belong mostly to crack formations only in the matrix, while for concrete with lower *w*/*c*, cracking occurs in both the matrix and aggregates.

Fig. 5 illustrates the characteristic frequency determined from waveform analysis of AE events during the splitting tests of mortars with different *w*/*c*. Fig. 5a shows the distribution of the maximum frequency of the waveforms (the frequency where the frequency spectrum has maximum amplitude) for the different mixtures. The detected AE waves are shown to have maximum frequency in three ranges including 100–150 kHz, 150–200 kHz, and 300–400 kHz. For *w*/*c* of 0.30, the number of AE events having maximum frequency between 300 kHz and 400 kHz increases dramatically and it will be asserted later in the paper that this range of maximum frequency may be attributed to acoustic emission due to aggregate cracking. AE events seen for all samples in the maximum frequency ranges between 100 kHz and 150 kHz and 150–200 kHz may belong to acoustic waves generated by matrix cracking, since matrix always participates in cracking in concrete fracture, regardless of its *w*/*c*.

The distributions of AE events versus waveform frequency center of gravity (FCG) are shown in Fig. 5b. Decreasing the *w*/*c*, the distribution moves to higher FCG ranges (300–400 kHz) which again is consistent with increased crack formation in the aggregate in lower *w*/*c* (higher strength concrete).

3.1.3. Constituent component response

Fig. 6 shows the cumulative distributions of AE energy and its derivative (probability density) as a function of the frequency center of gravity (FCG) of each AE event for samples prepared from

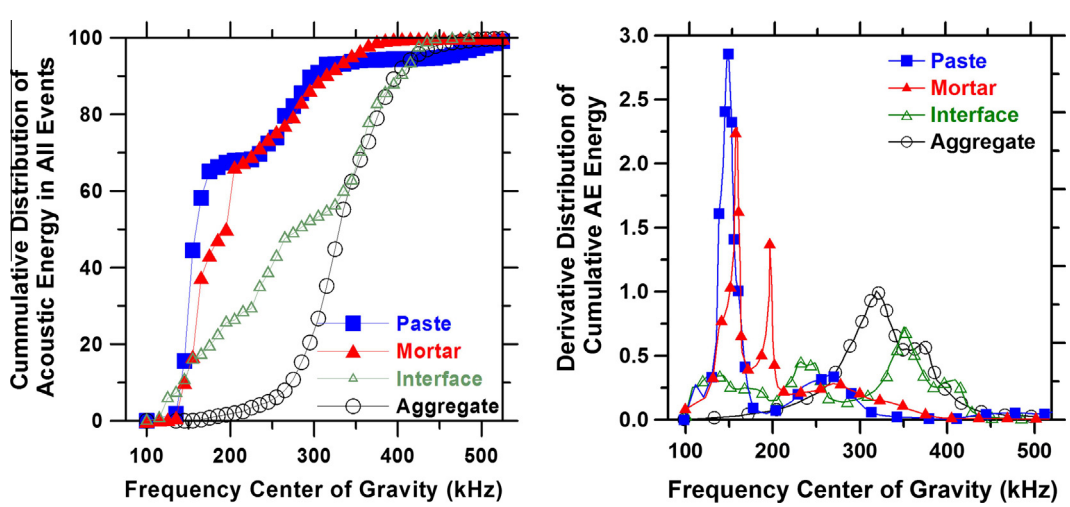

Fig. 6. Cumulative distribution of acoustic emission energy (left) and its derivative (right) versus frequency center of gravity for different components of concrete with comparison to the result for the mortar sample with a *w*/*c* of 0.42.

aggregate (Series II), paste (Series III), and interface (Series IV) wedge splitting tests, as well as the result of the wedge splitting test of the mortar with a *w*/*c* of 0.42. A large portion of the detected AE events due to cracking in aggregate was observed in the FCG range between 300 kHz and 400 kHz, which correlates with damage observed in the concrete samples prepared with different *w*/*c* discussed in the previous section. For paste samples, two ranges of FCG having higher levels of AE energy can be seen: (a) FCG around 150 kHz which encompasses 70% of the total detected energy, and (b) FCG around 250 kHz having 20% of the total energy. For ITZ cracking, the AE energy is approximately dispersed throughout the entire range of FCG. The cumulative distribution of AE energy for the mortar sample is relatively similar to that for the paste sample.

Comparing the results in Fig. 6 with the results in Fig. 5, it can be verified that first, aggregate cracking generates acoustic activity possessing higher frequencies (300–400 kHz), second, cracking in the matrix (paste and ITZ) mostly produces acoustic waves possessing lower frequencies (100–300 kHz).

3.2. Alkali silica reaction test

The second portion of this study examined the acoustic activity that occurs in samples undergoing alkali silica reaction. Available alkalis in concrete pore solution can react with reactive siliceous aggregates in the presence of water. This reaction is relatively slow and results in the development of an expansive gel that is formed over time. The expansion generated by the formation of ASR gel can result in the development of internal tensile stress in the aggregate and matrix. If this internal stress exceeds the strength of the aggregate or matrix, it can cause cracking. It has been suggested that cracking begins as microcracks that develop in the aggregate which, as the damage continues to occur, can extend into the matrix (i.e., the cement paste and ITZ) [32–34].

3.2.1. Length change and acoustic activity response

Fig. 7a shows the typical length change measurements for ASTM C490 samples stored in a 1 N NaOH solution at 23 °C ± 1 °C. It can be noticed that a similar (and minor) expansion occurs for both samples made with reactive and non-reactive aggregates up to 15 d. After this age, the rate of expansion begins to increase for samples made with reactive aggregate. It can be noticed that the samples made with reactive sand show an expansion of 0.1% after 72 d, while samples prepared with non-reactive sand show approximately 0.01% expansion throughout the duration of the test. It should be noted that the average coefficient of variation for length change measurement was respectively 21% for reactive aggregate and 13% for non-reactive aggregate.

Fig. 7b shows cumulative AE signal strength for samples prepared for AE detection with reactive and non-reactive sand. The difference between AE signal strength between the samples with reactive and non-reactive samples can be seen in this figure. Differences in the AE signal strength between reactive and non-reactive samples begins to diverge at 5 d and become more prevalent over time, while length change measurements (Fig. 7a) take a longer period (15 d) to show a difference between the non-reactive and reactive aggregates. In addition, the first dramatic change in AE signal strength (i.e., ASR cracking) can be observed at 26 d. According to the ASTM length change measurements, however, the reactivity of aggregate can be confirmed at 72 d. This illustrates the capability of AE to detect ASR cracking at early ages since it detects the onset of cracking, while it can take significantly longer using ASTM standard length change measurements, as the latter measures the influence of cracks on the length change. This is well investigated previously in the work done by Pour-Ghaz et al. [20].

AE activities for both samples are indicated in Fig. 8. While samples prepared using the non-reactive sand showed relatively few AE activities and substantially lower AE signal strength, samples prepared using the reactive sand indicated substantial amounts of AE activity and AE signal strength.

The AE activity detected at early ages in samples prepared using non-reactive aggregate (Fig. 8a) and some part of the early age AE activity in samples prepared using reactive aggregate (Fig. 8b) may be attributed to the absorption of NaOH solution or removal of air bubbles from the solution/sample. Samples prepared using the reactive aggregates showed several bursts of cracking events as well as more gradual AE activity developed over time. This appears to indicate that not only is ASR cracking a gradual fracturing, but it may be associated with specific discrete activities (instabilities) where numerous cracking events happen over a short period of time. These bursts of AE activities are highlighted by arrows in Fig. 8b.

3.2.2. Waveform analysis of ASR cracking

As previously mentioned, the aggregate is expected to crack before cracking occurs in the matrix [32–34]. And because aggregate typically cracks at a higher frequency, one would expect the earliest acoustic events in the ASR specimens to have higher frequency content than those occurring at later ages. Fig. 9 shows the number of AE events and their signal strength as a function of the frequency center of gravity for the AE waveforms in the reactive and non-reactive aggregate samples. Fig. 9a provides data to illustrate that the center of gravity of the frequency for the AE

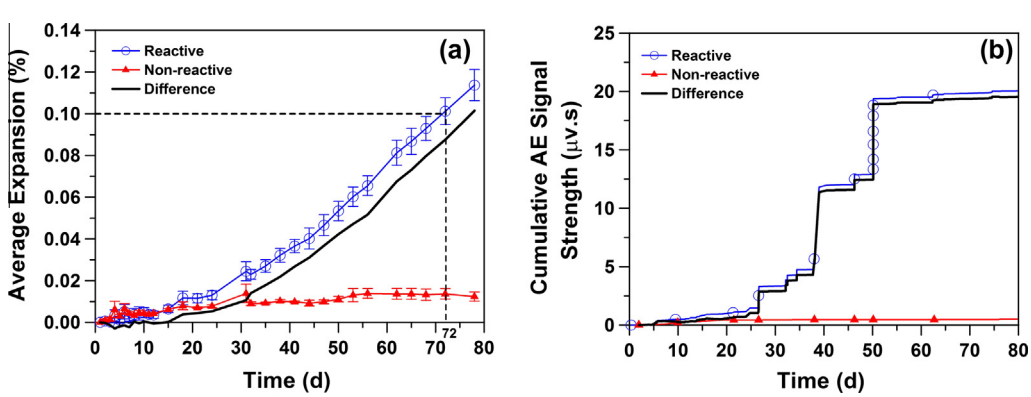

Fig. 7. (a) Length change of ASTM C490 mortar bars in 1 N NaOH at 23 °C ± 1 °C solution over time, (the error bars indicate ± one standard deviation for four replicates of length change measurement); and (b) cumulative AE signal strength for samples immersed in 1 N NaOH at 23 °C ± 1 °C solution over time (the differences in values between non-reactive and reactive samples are indicated with black line).

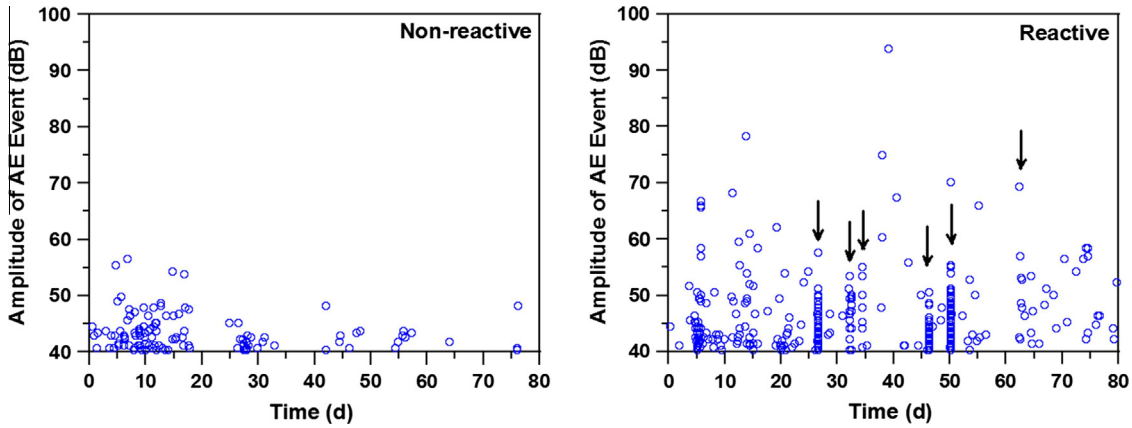

Fig. 8. Acoustic emission activity for samples prepared with reactive and non-reactive sand immersed in a 1 N NaOH solution at 23 °C ± 1 °C versus time (arrows show bursts of AE activity due to cracking).

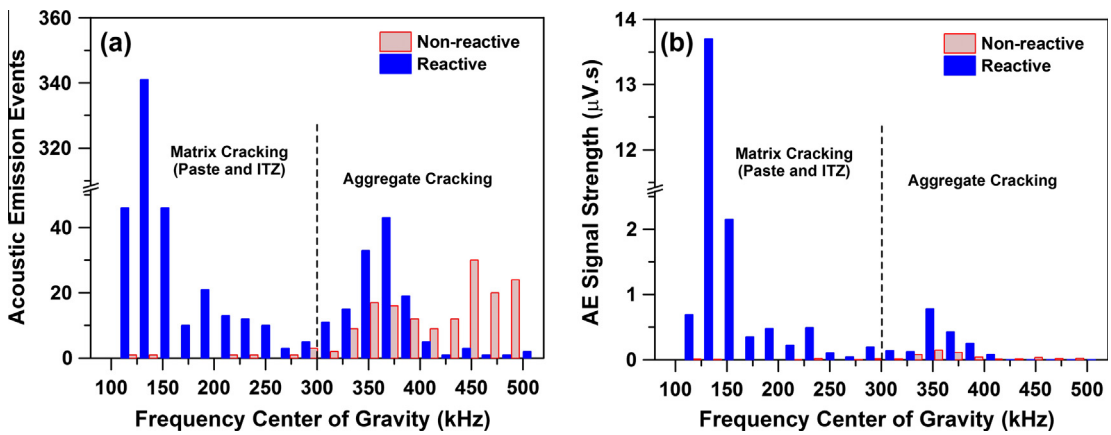

Fig. 9. Acoustic emission activity of ASR cracking in samples with reactive and non-reactive aggregates immersed in 1 N NaOH at 23 °C for 80 d: (a) distribution of AE events versus frequency center of gravity, and (b) distribution of AE signal strength versus frequency center of gravity (note that *y*-axis is clipped between 50 events and 310 events for (a), and between 2.5 μV s and 11.5 μV s for (b) to better illustrate the distribution).

events that were detected in the non-reactive samples tends to occur over the full range of frequencies with a slightly higher number of events occurring at higher frequencies which is consistent with aggregate cracking. These events, however, are relatively few in number and have very little AE signal strength (Fig. 9b). In contrast, the samples made with the reactive aggregates show AE events with differing frequencies (Fig. 9a and b). The center of gravity for the frequency in the samples made with reactive aggregates can be divided into two ranges: (a) low frequency range (100–300 kHz), which is consistent with matrix cracking occurring, and (b) higher frequency range (300–400 kHz) which is consistent with aggregate cracking.

To better understand how the cracking changes as a function of time, Fig. 10 was developed to plot the number of AE events versus the center of gravity for the frequency in samples with non-reactive (Fig. 10a) and reactive aggregates (Fig. 10b) during three different time ranges: early exposure time (1–21 d), moderate exposure time (22–42 d), and long-term exposure time (after 43 d). It can be noticed that the samples prepared with the non-reactive aggregate have events that are predominantly located in the same frequency ranges at all exposure ages. As mentioned before, the corresponding cumulative AE signal strength for these events was found to be very small (Fig. 10b). The samples with the reactive aggregate have waves that initially (1–21 d) occur predominantly at the higher frequency range (300–400 kHz) which would be consistent with aggregate cracking due to stresses caused by ASR gel expansion inside aggregate, and over time an increasing portion of the acoustic activity shifts to the lower frequencies (100–300 kHz) which would be consistent with more matrix (ITZ and paste) cracking.

The results observed for ASR cracking (Figs. 9 and 10) match almost completely with the results obtained in mechanical wedge splitting tests for aggregate and matrix cracking (Figs. 5 and 6).

In addition to AE waveform signatures such as AE events, peak amplitude, AE energy, AE signal strength, rise time, duration, maximum frequency, and frequency center of gravity, other AE indices have been used in an attempt to help classify the cracks, as has been done in other literature [25–27,46]. RA value (rise time/amplitude) and average frequency (AF) are two AE indices which are used to distinguish tensile and shear cracks [25–27,46]. The RA index and AF index can be calculated using Eqs. (2) and (3), respectively.

$$RA = \frac{RT}{A} \tag{2}$$

$$AF = \frac{C}{D} \tag{3}$$

where RT is the rise time (the delay time between the onset of an AE waveform and the peak amplitude), A is peak amplitude, D is the duration of an AE waveform (the time between the first and the last threshold crossing), and C is the total number of threshold crossings

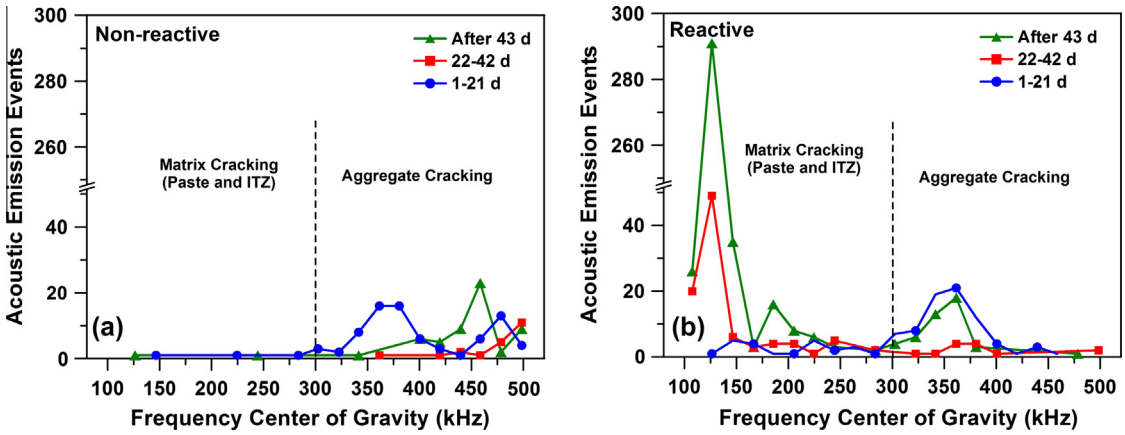

Fig. 10. Distribution of AE events at different periods of time versus frequency center of gravity for mortar sample with reactive and non-reactive aggregate immersed in 1 N NaOH at 23 °C (note that *y*-axis was clipped between 50 events and 250 events to better illustrate the distribution).

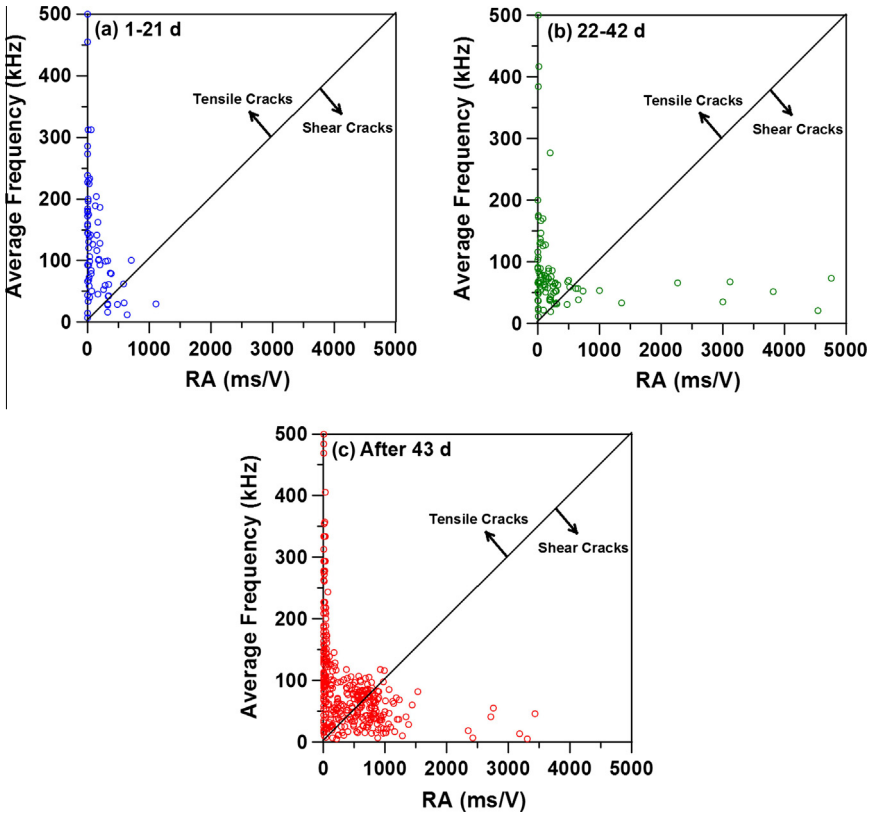

Fig. 11. Average frequency (AF) versus RA index for ASR AE events of samples prepared by reactive aggregates during (a) 1–21 d, (b) 22–42 d, and (c) after 43 d.

for an AE waveform [27]. By means of the RA and AF indices, cracks can be classified into tensile and shear cracks [25–27,46]. Fig. 11 shows average frequency versus RA index during three different time ranges as before: early exposure time (1–21 d), moderate exposure time (22–42 d), and long-term exposure time (after 43 d). The commonly suggested slope for the line to separate tensile cracking and shear cracking is 0.1 Hz s/V, which was obtained based on four-point bending tests and the direct shear tests of concrete specimens [25–27,46]. When the ratio of AF to RA for an AE event becomes greater than 0.1 Hz s/V, this AE event can be considered as an acoustic activity for tensile cracking. Similarly, AE events with the AF to RA ratios less than 0.1 Hz s/V can be considered as acoustic activities for shear cracking. It should be mentioned that when this ratio is close to 0.1 Hz s/V, the cracking can be a combination of shear and tensile cracking [25–27,46].

During early exposure times (Fig. 11a), most of the AE events are predominantly located within the upper half part of the AF versus RA plot which can indicate that tensile cracks are forming. This is consistent with the fact that tensile micro-cracks occur inside aggregate at early ages in ASR tests due to the expansion of the newly formed ASR gel. At moderate exposure times (Fig. 11b), some AE activities begin to correspond with shear cracking which may represent the initiation of crack extension to the matrix (ITZ and cement paste); tensile cracks are still observed due to additional tensile cracking caused by the ASR gel and aggregate expansion. At later exposure times

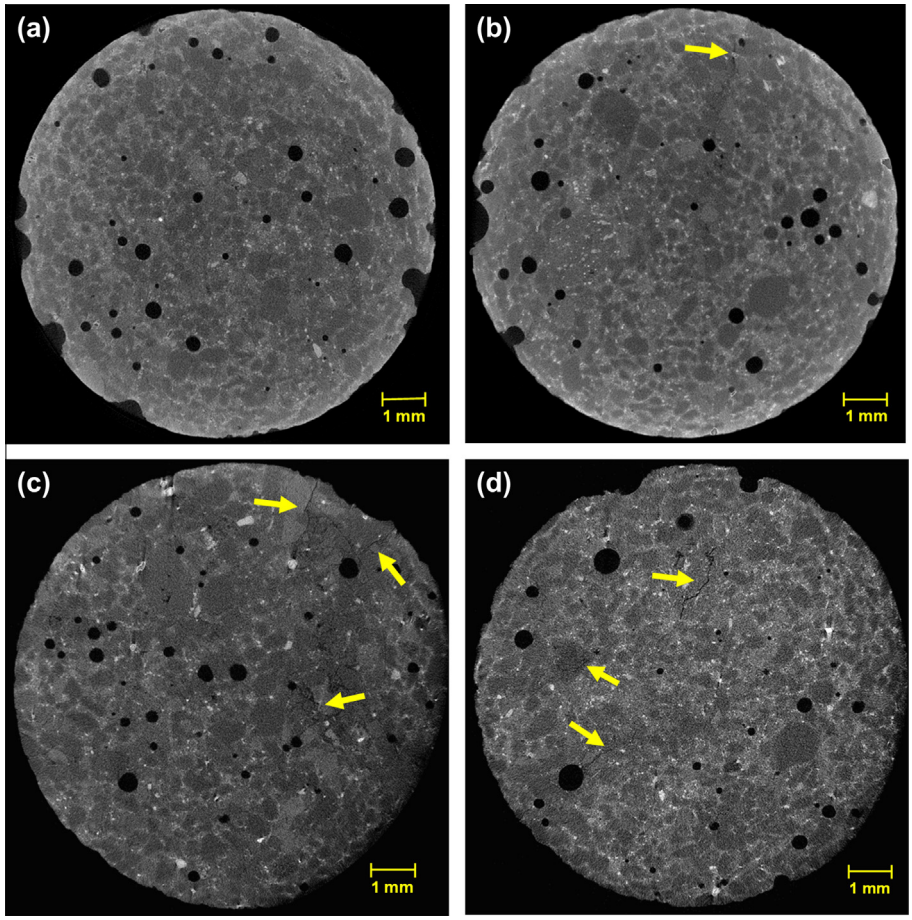

Fig. 12. X-ray tomography of mortar samples immersed in 1 N NaOH at 23 °C: (a) initial imaging: no cracking, (b) 44 d: initiation of visual cracks, (c) 89 d: propagation of cracks into ITZ and paste, and (d) 116 d: growth of cracks (arrows highlight cracking in the mortar specimens).

(Fig. 11c), a combination of tensile and shear cracking can be observed which shows the formation of cracks in aggregate, ITZ, and cement paste. It should be mentioned that the aggregate cracking in ASR tests may most likely be the tensile cracking, while the matrix (ITZ and cement paste) cracking may most likely be the shear cracking [32–34].

3.2.3. Analysis of X-ray computed tomography images

In addition to length change measurement and AE recording for ASR samples, X-ray computed tomography was also performed to relate physical damage to length change and AE measurements. Fig. 12 shows X-ray computed tomography images (2-D) for samples with reactive aggregate after different durations of being exposed to the 1 N NaOH solution. During early ages before 44 d, the X-ray computed tomography images remain almost unchanged and no cracking was observed; this might be due to the image resolution which does not permit detection of micro-cracking which is expected to occur in the aggregate. The first visual cracking was detected at 44 d (Fig. 12b). At this age, samples with reactive aggregate showed a relatively considerable length change (Fig. 7a). According to AE measurement, moreover, this cracking is associated with detection of numerous amounts of AE events at different frequency ranges which indicates the formation of cracks and macro-cracks due to fracture in aggregate and matrix. At later ages, more cracking is observed in the matrix and through the aggregates in the samples (Fig. 12c and d) showing the progression of ASR cracking. Although initial cracking was not able to be observed with the specimen size and instrument settings, higher resolution scanners are available that could be able to provide insightful observations [32,47].

4. Conclusions

This work has shown that acoustic emission (AE) is an experimental technique that is capable of detecting cracking in concrete and the frequency of the AE events may be used to determine which component of concrete is cracking. The AE activity due to concrete cracking can be divided into two main categories: (1) a high frequency range AE event (between 300 kHz and 400 kHz) which can be an indication of aggregate cracking, and (2) a low frequency range AE event (between 100 kHz and 300 kHz) which can be an indication of matrix cracking (paste and ITZ). The frequency ranges were determined by performing wedge splitting tests on specific specimens of (1) rock, (2) hydrated cement paste, (3) composite samples which are a combination of rock and hydrated cement paste, and (4) mortar samples.

ASR tests were also performed on samples with reactive and non-reactive aggregates, with concurrent AE measurements. Substantially greater acoustic activity was observed for samples with reactive aggregate than in samples with non-reactive aggregates. Samples with reactive aggregate showed acoustic activity long before significant expansion occurred. Comparing the results from the length change measurement and AE detection for ASR testing, acoustic emission may be used as a technique to detect the reactivity of the aggregate faster than the common length change measurements; however, more research needs to be done.

For the ASR experiment in this study, it was also found that the frequency of AE events varies during different exposure ages due to the fact that (1) at early ages, cracking begins in the aggregates, and (2) at later ages, the cracking develops to the matrix. Aggregate cracking (early age evidence) had a high frequency range, while matrix cracking (later age evidence) showed a low frequency range that was consistent with the results obtained in mechanical wedge splitting tests for aggregate and matrix cracking. AE indices (i.e., rise time/amplitude value and average frequency) were also obtained for ASR tests and a fairly good agreement was observed between the rise time/amplitude and average frequency response to define the mode of failure (tension vs. shear). At early exposure ages, tensile cracks were observed due to tensile aggregate cracking, while a combination of tensile and shear cracking was seen at later exposure ages due to aggregate and matrix cracking.

X-ray computed tomography, at the resolution employed in this study (3.9 μm × 3.9 μm × 3.9 μm), partially supports the results obtained from AE measurement and it was able to detect ASR cracking no sooner than 44 d. At later ages, visible cracks were detected using X-ray computed tomography due to extension and growth of ASR micro-cracks. X-ray computed tomography with a higher resolution (or smaller voxel size) may be needed to observe the ASR micro-cracking at early ages.

Acknowledgements

Part of this research was performed while one of the authors was a visiting professor at the Technical University of Denmark, funded by the Knud Højgaard Foundation. The authors gratefully acknowledge the assistance of Max Peltz for his help with ASR sample preparation. The authors also wish to thank Kevin Folliard and Mike Thomas for insightful discussion on ASR.

References

[1] Sih GC, DiTommaso A. Fracture mechanics of concrete: structural application and numerical calculation. Netherlands, Dordrecht: Springer; 1984. http://dx.doi.org/10.1007/978-94-009-6152-4.
[2] Li Z, Shah SP. Localization of microcracking in concrete under uniaxial tension. ACI Mater J 1994;91:372–81.
[3] Pour-Ghaz M. Detecting damage in concrete using electrical methods and assessing moisture movement in cracked concrete. Purdue University; 2011.
[4] Yang Z. Assessing cumulative damage in concrete and quantifying its influence on life cycle performance modeling. Purdue University; 2004.
[5] Pour-Ghaz M, Weiss J. Detecting the time and location of cracks using electrically conductive surfaces. Cem Concr Compos 2011;33:116–23. http://dx.doi.org/10.1016/j.cemconcomp.2010.09.015.
[6] Pour-Ghaz M, Weiss J. Application of frequency selective circuits for crack detection in concrete elements. J ASTM Int 2011;8. http://dx.doi.org/10.1520/JAI103826.
[7] Pour-Ghaz M, Poursaee A, Spragg R, Weiss J. Experimental methods to detect and quantify damage in restrained concrete ring specimens. J Adv Concr Technol 2011;9:251–60. http://dx.doi.org/10.3151/jact.9.251.
[8] Landis EN, Shah SP. Frequency-dependent stress wave attenuation in cement-based materials. J Eng Mech 1995;121:737–43. 10.1061/(ASCE)0733-9399(1995) 121:6(737).
[9] Pour-Ghaz M, Rajabipour F, Couch J, Weiss J. Numerical and experimental assessment of unsaturated fluid transport in saw-cut (notched) concrete elements. ACI Spec Publ 2009;266:73–86.
[10] Landis EN, Baillon L. Experiments to relate acoustic emission energy to fracture energy of concrete. J Eng Mech 2002;128:698–702. http://dx.doi.org/10.1061/(ASCE)0733-9399(2002) 128:6(698).
[11] Yoon D-J, Weiss WJ, Shah SP. Detecting the extent of corrosion with acoustic emission. Transport Res Rec 2000:54–60. <http://cat.inist.fr/?aModele=afficheN&cpsidt=798502> [accessed 21.03.13].
[12] Ohtsu M. Nondestructive evaluation of damaged concrete due to freezing and thawing by elastic-wave method. J Adv Concr Technol 2005;3:333–41. http://dx.doi.org/10.3151/jact.3.333.
[13] Farnam Y, Bentz D, Sakulich A, Flynn D, Weiss J. Measuring freeze and thaw damage in mortars containing deicing salt using a low-temperature longitudinal guarded comparative calorimeter and acoustic emission. Adv Civ Eng Mater 2014;3:316–37. http://dx.doi.org/10.1520/ACEM20130095.
[14] Farnam Y, Bentz D, Hampton A, Weiss J. Acoustic emission and low temperature calorimetry study of freeze and thaw behavior in cementitious materials exposed to sodium chloride salt. Transport Res Rec 2014;2441:81–90.
[15] Saliba J, Loukili A, Grondin F, Regoin JP. Identification of damage mechanisms in concrete under high level creep by the acoustic emission technique. Mater Struct 2013;47:1041–53. http://dx.doi.org/10.1617/s11527-013-0113-6.
[16] Rossi P, Godart N, Robert JL, Gervais JP, Bruhat D. Investigation of the basic creep of concrete by acoustic emission. Mater Struct 1994;27:510–4. http://dx.doi.org/10.1007/BF02473211.
[17] Farnam Y, Todak H, Spragg R, Weiss J. Electrical response of mortar with different degrees of saturation and deicing salt solutions during freezing and thawing. Cem Concr Compos 2015;59:49–59. http://dx.doi.org/10.1016/j.cemconcomp.2015.03.003.
[18] Farnam Y, Wiese A, Bentz D, Davis J, Weiss J. Damage development in cementitious materials exposed to magnesium chloride deicing salt. Constr Build Mater; 2015 [in press].
[19] Qian Y, Farnam Y, Weiss J. Using acoustic emission to quantify freeze–thaw damage of mortar saturated with NaCl solutions. In: Proc 4th int conf durab concr struct. Purdue University Libraries Scholarly Publishing Services; 2014. p. 32–7. http://dx.doi.org/10.5703/1288284315379.
[20] Pour-ghaz M, Spragg R, Castro J, Weiss J. Can acoustic emission be used to detect alkali silica reaction earlier than length change? In: 14th int conf alkali-aggregate react. Austin (Texas): University of Texas; 2012. p. 1–10.
[21] Vallen H. AE testing fundamentals, equipment, applications. Nondestruct Test 2002;7. <www.NDT.net>.
[22] Puri S, Weiss J. Assessment of localized damage in concrete under compression using acoustic emission. J Mater Civ Eng 2006;18:325–33. http://dx.doi.org/10.1061/(ASCE)0899-1561(2006)18:3(325).
[23] Yuyama S, Li Z, Ito Y, Arazoe M. Quantitative analysis of fracture process in RC column foundation by moment tensor analysis of acoustic emission. Constr Build Mater 1999;13:87–97. http://dx.doi.org/10.1016/S0950-0618(99)00011-2.
[24] Shigeishi M, Ohtsu M. Acoustic emission moment tensor analysis: development for crack identification in concrete materials. Constr Build Mater 2001;15:311–9. http://dx.doi.org/10.1016/S0950-0618(00)00079-9.
[25] Ohtsu M, Isoda T, Tomoda Y. Acoustic emission techniques standardized for concrete structures. J Acoust Emiss 2007;25:21–32.
[26] Ohno K, Ohtsu M. Crack classification in concrete based on acoustic emission. Constr Build Mater 2010;24:2339–46. http://dx.doi.org/10.1016/j.conbuildmat.2010.05.004.
[27] Aggelis DG. Classification of cracking mode in concrete by acoustic emission parameters. Mech Res Commun 2011;38:153–7. http://dx.doi.org/10.1016/j.mechrescom.2011.03.007.
[28] Pollock AA. Material brittleness and the energetics of acoustic emission. In: Proulx T, editor. Exp Mech Emerg Energy Syst Mater (Proceedings Soc Exp Mech Ser 16), vol. 5. New York (NY): Springer New York; 2011. p. 73–9. http://dx.doi.org/10.1007/978-1-4419-9798-2.
[29] Prosser WH, Jackson KE, Kellas S, Smith BT, Mckeon J, Friedman A. Advanced, waveform based acoustic emission detection of matrix cracking in composites. Mater Eval 1995;53:1052–8.
[30] Zdunek AD, Prine DW, Li Z, Landis E, Shah SP. Early detection of steel rebar corrosion by acoustic emission monitoring. In: Corros 95 NACE int annu conf corros show. NACE International; 1995. p. 1–9.
[31] Schumacher T, Straub D, Higgins C. Toward a probabilistic acoustic emission source location algorithm: a Bayesian approach. J Sound Vib 2012;331:4233–45. http://dx.doi.org/10.1016/j.jsv.2012.04.028.
[32] Winter N. Understanding cement: introduction to Portland cement production, cement and concrete chemistry and deleterious processes in concrete. WHD Microanalysis Consultants Ltd.; 2012.
[33] Chatterji S, Thaulow N, Jensen AD. Studies of alkali–silica reaction. Part 5. Verification of a newly proposed reaction mechanism. Cem Concr Res 1989;19:177–83. http://dx.doi.org/10.1016/0008-8846(89)90081-1.
[34] Chatterji S, Thaulow N, Jensen AD. Studies of alkali–silica reaction, part 6. Practical implications of a proposed reaction mechanism. Cem Concr Res 1988;18:363–6. http://dx.doi.org/10.1016/0008-8846(88)90070-1.
[35] NT BUILD 201. Concrete: making and curing of moulded test. In: Nord. METHOD. Oslo, Norway: Nordic Innovation Centre; 1984. p. 1–6.
[36] Hodicky K, Hulin T, Schmidt JW, Stang H. Wedge splitting test on fracture behaviour of fiber reinforced and regular high performance concretes. In: 13th int conf fract; 2013. p. 1–10.
[37] NT BUILD 511. Wedge splitting test method (WST): fracture testing of fibre-reinforced concrete (Mode I). In: Nord. METHOD. Oslo, Norway: Nordic Innovation Centre; 2005. p. 1–6.
[38] ASTM. ASTM C1260-Standard test method for potential alkali reactivity of aggregates (mortar-bar method). In: ASTM Int. West Conshohocken (PA): ASTM International; 2012. p. 1–5. <http://scholar.google.com/scholar?hl=en&btnG=Search&q=intitle:Standard+Test+Method+for+Potential+Alkali+Reactivity+of+Aggregates+(+Mortar-Bar#1> [accessed 21.03.13].
[39] ASTM. ASTM C778 – standard specification for standard sand. West Conshohocken (PA): ASTM International; 2013.
[40] ASTM. ASTM C136 – standard test method for sieve analysis of fine and coarse aggregates. West Conshohocken (PA): ASTM International; 2013.
[41] ASTM. ASTM C305 – standard practice for mechanical mixing of hydraulic cement pastes and mortars of plastic consistency. West Conshohocken (PA): ASTM International; 2012. http://dx.doi.org/10.1520/C0305-12.
[42] ASTM. ASTM C490 – standard practice for use of apparatus for the determination of length change of hardened cement paste, mortar, and concrete. West Conshohocken (PA): ASTM International; 2011.

[43] Shah SP, Swartz SE, Ouyang C. Fracture mechanics of concrete: applications of fracture mechanics to concrete, rock and other quasi-brittle materials. New York (NY): Wiley; 1995.
[44] Mehta PK, Monteiro PJ. Concrete: microstructure, properties, and materials. 3rd ed. New York: McGraw-Hill; 2005.
[45] Powers TC, Brownyard TL. Studies of the physical properties of hardened Portland cement paste. In: PCA Res Dep Bull 22. Chicago: Portland Cement Association; 1948.
[46] Ono K. Application of acoustic emission for structure diagnosis. In: Michalski R, editor. Diagnostics Struct Heal Monit. Polskie Towarzystwo Diagnostyki Technicznej; 2011. p. 3–18.
[47] Olek J, Kim T, Pour-Ghaz M, Farnam Y, Chiu Y-C, Balachandran C, et al. Alkali–silica reaction (ASR) mechanisms and detection: an advanced understanding. Federal Highway Administration, FHWA-HRT-14-078; 2013.